

A region of high-spin toroidal isomers

Andrzej Staszczak^{a,*}, Cheuk-Yin Wong^b

^a*Institute of Physics, Maria Curie-Skłodowska University, pl. M. Curie-Skłodowskiej 1, 20-031 Lublin, Poland*

^b*Physics Division, Oak Ridge National Laboratory, P.O. Box 2008, Oak Ridge, Tennessee 37831, USA*

Abstract

The combined considerations of both the bulk liquid-drop-type behavior and the quantized angular momentum reveal that high-spin toroidal isomeric states may have general occurrences for light nuclei with $28 \leq A \leq 48$. High-spin $N=Z$ toroidal isomers in this mass region have been located theoretically using cranked self-consistent constraint Skyrme-Hartree-Fock model calculations.

Keywords: Toroidal light nuclei, High K-isomeric states

PACS: 21.60.Jz, 21.60.Ev, 23.35.+g, 27.40.+t, 27.40.+z

Nuclei as we now know them have sphere-like geometry. Wheeler suggested that under appropriate conditions the nuclear fluid may assume a toroidal shape [1, 2, 3]. Toroidal nuclei are however plagued with various instabilities [3], and the search remains elusive [4, 5, 6]. It was found previously from the liquid-drop model that a “rotation” about the symmetry axis with an angular momentum $I=I_z$ above a threshold can stabilize the toroidal nucleus and can lead to a high-spin isomer [7].

The toroidal high-spin isomer, whose large angular momentum $I=I_z$ must be generated by the alignment of individual nucleon angular momenta along the symmetry axis [8], provides an elegant example in quantum mechanics as how an axially-symmetric system can acquire a quantized angular momentum. Furthermore, the nuclear fluid in the toroidal isomeric state may be so severely distorted by the change from sphere-like geometry to the toroidal shape that it may acquire bulk properties of its own, to make it a distinct type of quantum fluid. Finally, the toroidal high-spin isomer may be a source of energy, as its decay to the ground state can release a large amount of excitation energy and the possibility of toroidal high-spin isomers may stimulate also future reaction studies to explore their production and detection by fusion of two ions at high angular momenta [9, 10]. For all these reasons, the investigation on toroidal high-spin isomers is of general interest.

In the liquid-drop model of a toroidal nucleus, we can select the major radius R , the minor radius d , the angular momentum $I=I_z$ about the symmetry axis, and the corresponding rigid-body moment of inertia $\mathfrak{I}_{\text{rigid}}$ as macroscopic variables. (For a sketch of R and d , see Fig. 1 of [3].) The energy $I(I+1)/2\mathfrak{I}_{\text{rigid}}$ associated with the angular momentum I can be called the “rotational” energy. The variation of the rotational energy and the Coulomb energy tend to counter-balance the variation of the surface energy [7]. As a consequence, there is an I -threshold above which the rotating toroidal nucleus can be stable against a variation of R/d . The toroidal nucleus is stable also against axially-asymmetric sausage distortions within an I -window, when the same mass flow is maintained across the toroidal meridian. Beyond the I -window, sausage instabilities of higher orders dominate to break the toroid into many beads [7].

To study toroidal high-spin states theoretically, we need a systematic way to determine the quantized I value, which is a non-trivial function of N and Z . The quantized I can be obtained from the single-particle state diagrams under the constraint of a fixed aligned angular momentum. For simplicity, we limit our present studies to even-even $N=Z$ nuclei. Previously, an investigation of ^{40}Ca as the evolution of a chain of 10 alpha particles revealed that ^{40}Ca with $I=60 \hbar$ may represents a toroidal high K-isomeric state [11], in qualitative agreement with the I -threshold and I -window concepts in [7].

Accordingly, we need the energy diagram of the single-particle states in a toroidal nucleus for different

*Corresponding author

Email addresses: stas@tytan.umcs.lublin.pl (Andrzej Staszczak), wongc@ornl.gov (Cheuk-Yin Wong)

aligned angular momenta I . For $I=0 \hbar$, the single-particle potential for a nucleon in a toroidal nucleus with azimuthal symmetry in cylindrical coordinates (r, z) can be represented by [3]

$$V_0(r, z) = \frac{1}{2}m\omega_0^2(r - R)^2 + \frac{1}{2}m\omega_0^2z^2, \quad (1)$$

where $\hbar\omega_0 = [(3\pi R/2d)^{1/3}41/A^{1/3}]\langle\rho_{\text{torus}}\rangle/\langle\rho_0\rangle$. We have included the ratio $\langle\rho_{\text{torus}}\rangle/\langle\rho_0\rangle$ where $\langle\rho_{\text{torus}}\rangle$ and $\langle\rho_0\rangle$ are the average nuclear densities in the toroidal and the spherical configurations respectively, because the mean-field potential is proportional approximately to the nuclear density. In microscopic calculations, $\langle\rho_{\text{torus}}\rangle/\langle\rho_0\rangle$ is found to be approximately 1/2 to 2/3. For $R \gg d$ and low-lying states with the radial nodal quantum number $n_\rho=0$ and the azimuthal nodal quantum number $n_z=0$, the expectation value of the spin-orbit interaction is approximately zero [3], and we can neglect the spin-orbit interaction.

We label a state by $(n\Lambda\Omega\Omega_z)$, where $n=(n_z + n_\rho)$, $\pm\Lambda$ is the z -component of the orbital angular momentum, and $\Omega = |\Lambda \pm 1/2|$ is the single-particle total angular momentum with z -components $\Omega_z = \pm\Omega$. For $R \gg d$, the single-particle energy of the $(n_\rho n_z \Lambda \Omega)$ state with $I=0 \hbar$ is therefore

$$E(n\Lambda\Omega) \sim \hbar\omega_0(n + 1) + \frac{\hbar^2\Lambda^2}{2mR^2}. \quad (2)$$

Fig. 1(a) gives the single-particle state energies as a function of R/d for a toroidal nucleus with $I=0 \hbar$.

For a non-collectively rotating toroidal nucleus with aligned angular momentum, $I=I_z$, we use a Lagrange multiplier ω to describe the constraint $I_z = \langle\hat{J}_z\rangle = \sum_{i=1}^N \Omega_{z,i}$. The constrained single-particle Hamiltonian becomes $\hat{h}' = \hat{h} - \omega\hat{J}_z$, and the aligned angular momentum I is a step-wise function of the Lagrange multiplier ω [12], with each I spanning a small region of $\hbar\omega$. As the constrained Hamiltonian \hat{h}' is of the same form as that of a nucleus under an external cranking, the constraint can be effectively described as a cranking of the nucleus with an angular frequency ω [13, 14]. The single-particle state energy of the $(n\Lambda\Omega\Omega_z)$ state, under the constraint of the non-collective aligned angular momentum I is

$$E(n\Lambda\Omega\Omega_z) \sim \hbar\omega_0(n + 1) + \frac{\hbar^2\Lambda^2}{2mR^2} - \hbar\omega\Omega_z. \quad (3)$$

Fig. 1(b) gives the single-particle state energies as a function of the constraining Lagrange multiplier $\hbar\omega$, for a toroidal nucleus with $R/d=4.5$, approximately the aspect ratio for many toroidal nuclei in this region. We can use Fig. 1(b) to determine $I=I_z$ as a function of N

and $\hbar\omega$. Specifically, for a given N and $\hbar\omega$, the aligned I_z -component of the total angular momentum I from the N nucleons can be obtained by summing $\Omega_{z,i}$ over all states below the Fermi energy.

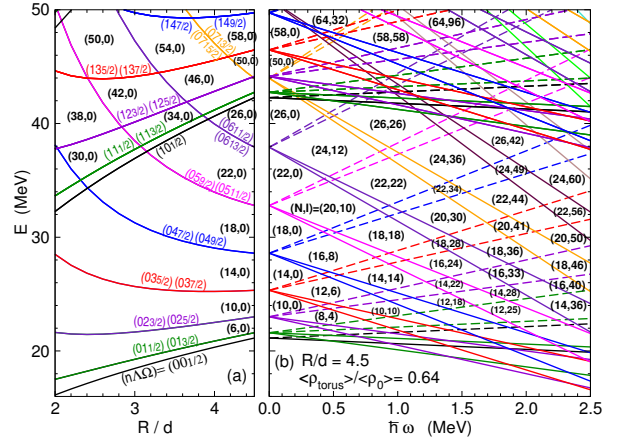


Figure 1: (Colour online.) (a) Single-particle states of a toroidal nucleus with $I=0 \hbar$ as a function of R/d , calculated with $\langle\rho_{\text{torus}}\rangle/\langle\rho_0\rangle=0.64$ and $A\sim 40$. Each state is labeled by (n, Λ, Ω) , with $n=n_z+n_\rho$ and degenerate Ω_z . (b) Single-particle states of a toroidal nucleus with $R/d=4.5$, as a function of a cranking frequency $\hbar\omega$. Energy levels of positive- and negative- Ω_z states are given by the solid and dashed lines, respectively. The listed pair numbers (N, I) refer to the occupation number N and the total angular momentum $I=I_z$ aligned along the symmetry z -axis.

There are shell gaps for different (N, I_z) configurations in Fig. 1. They represent configurations with relative stability for which additional shell corrections on top of the liquid-drop-type energy surface [15, 3] may enhance the stability for toroidal configurations. The energy scales of the $\hbar\omega$ and E axes in Fig. 1(b) depend on N , R/d , $\langle\rho_{\text{torus}}\rangle/\langle\rho_0\rangle$ which vary individually at different isomeric toroidal energy minima, but the structure of the (N, I_z) shells and their relative positions in Fig. 1(b) remain approximately the same in this $A\sim 40$ mass region. We can use Fig. 1(b) as a qualitative guide to explore the landscape of the energy surface for different (N, I_z) configurations, by employing a reliable microscopic model.

A microscopic theory that includes both the single-particle shell effects and the bulk properties of a nucleus is the Skyrme energy density functional approach in which we solve an equality-constrained problem:

$$\left\{ \begin{array}{l} \min_{\hat{\rho}} E^{\text{tot}}[\hat{\rho}] \\ \text{subject to: } \langle \hat{N}_q \rangle = N_q, \\ \quad \langle \hat{Q}_{\lambda\mu} \rangle = Q_{\lambda\mu}, \\ \quad \langle \hat{J}_i \rangle = I_i, \end{array} \right. \quad (4)$$

where an objective function, $E^{\text{tot}}[\bar{\rho}] = \langle \hat{H}_{Sk} \rangle$, is the Skyrme energy density functional [16]. The constraint functions are defined by average values of the proton/neutron particle-number operator, $\hat{N}_{p/n}$, the mass-multiple-moment operators, $\hat{Q}_{\lambda\mu}$, and the components of the angular momentum operator \hat{J}_i . $N_{p/n} = Z/N$ are the proton/neutron numbers, $Q_{\lambda\mu}$ are the constraint values of the multiple-moments, and I_i are the constraint components of the angular momentum vector.

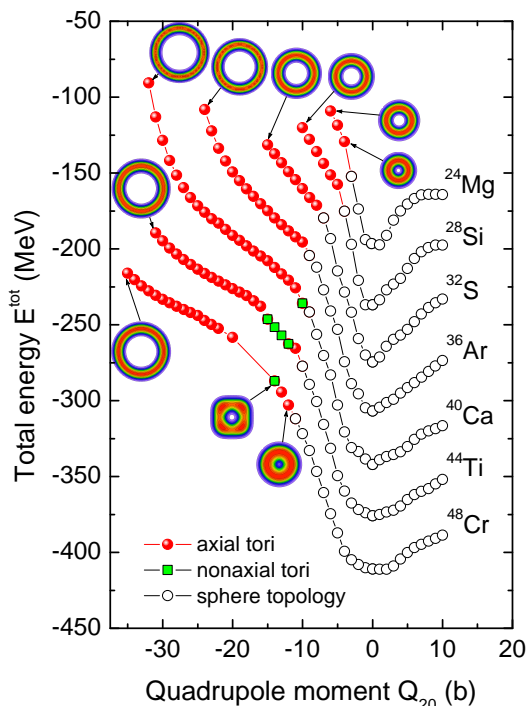


Figure 2: (Colour online.) The total HFB energy of ^{24}Mg , ^{28}Si , ^{32}S , ^{36}Ar , ^{40}Ca , ^{44}Ti , and ^{48}Cr as a function of the quadrupole moment for the case of $I=0$. Axially-symmetric toroidal configurations are indicated by the solid bullet points, axially-asymmetric toroidal configurations by squared points, and configurations with the topology of a sphere by open circles. Some toroidal density distributions are displayed.

The above constraint equations were solved using an augmented Lagrangian method [17] with the symmetry-unrestricted code HFODD [18]. In the particle-hole channel the Skyrme SkM* force [19] was applied and a density-dependent mixed pairing [20, 21] interaction in the particle-particle channel was used. The code HFODD uses the basis expansion method in a

three-dimensional Cartesian deformed harmonic oscillator basis. In the present study, we used the basis which consists of states having not more than $N_0=26$ quanta in the Cartesian directions, and not more than 1140 states.

Our objective is to locate local toroidal figures of equilibrium, if any, in the multi-dimensional search space of (A, Q_{20}, I) . We first map out the energy landscape for axially-symmetric toroidal shapes under these Q_{20} and I constraints, with fine grids in Q_{20} and all allowed non-collective rotations in $0 \leq I \leq 120 \hbar$ for different A . If the topographical landscape reveals a local energy minimum then the quadrupole constraint is removed at that minimum and free-convergence is tested to ensure that the non-collectively rotating toroid nucleus is indeed a figure of equilibrium.

For the case of $I=0$, as shown in Fig. 2, the Skyrme-Hartree-Fock-Bogoliubov (HFB) calculations for $N=Z$ with $24 \leq A \leq 48$ reveal that as the quadrupole moment constraint, Q_{20} , decreases to become more negative, the density configurations with sphere-like geometry (open circular points) turn into those of an axially-symmetric torus (solid bullet points), as would be expected from the single-particle state diagrams of Fig. 1(a). The energies of axially-symmetric toroidal configurations as a function of Q_{20} lie on a slope. This indicates that even though the shell effects cause the density to become toroidal when there is a quadrupole constraint, the magnitudes of the shell corrections are not sufficient to stabilize the tori against the bulk tendency to return to sphere-like geometry.

We next extend our Skyrme-HFB calculations further to include both the quadrupole moment Q_{20} constraint and the angular momentum constraint, $I=I_z$. The pairing energies are smaller for toroidal nuclei than with a spherical geometry, for a case of $I=0$, additionally pairing interaction is suppressed as the two degenerate $\pm\Omega_z$ states split apart under the constraining $\hbar\omega$ when $I \neq 0$. We shall carry out the cranking calculations without the pairing interaction, using a Skyrme-HF approach. The results of such calculations for $28 \leq A \leq 48$ are presented in Fig. 3, where we plot the excitation energy of the high-spin toroidal states relative to the spherical ground state energy, $E^* = E^{\text{tot}}(I) - E_{\text{g.s.}}^{\text{tot}}(0)$, as a function of the constrained Q_{20} , for different quantized I . For each point (Q_{20}, I) on an I curve for a fixed A , it was necessary to adjust $\hbar\omega$ judiciously within a range to ensure that the total aligned angular momentum of all nucleons in the occupied states gives the quantized I value of interest. The energy curves in Fig. 3 become flatter as I increases, similar to the energy curves in the liquid-drop model as the angular momentum increases [7].

With our systematic method outlined above, we are

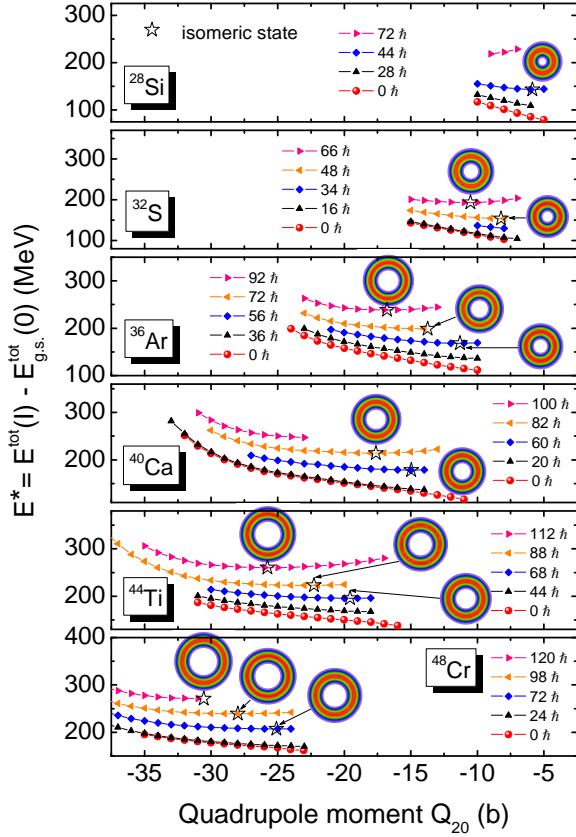


Figure 3: (Colour online.) The excitation energy of high-spin toroidal states (E^*) of ^{28}Si , ^{32}S , ^{36}Ar , ^{40}Ca , ^{44}Ti , and ^{48}Cr as a function of Q_{20} for different angular momentum along the symmetry axis, $I=I_z$. The density distributions and locations of isomeric toroidal energy minima are indicated by the star symbols.

able to locate many high-spin toroidal isomeric states: $^{28}\text{Si}(I=44 \hbar)$, $^{32}\text{S}(I=48, 66 \hbar)$, $^{36}\text{Ar}(I=56, 72, 92 \hbar)$, $^{40}\text{Ca}(I=60, 82 \hbar)$, $^{44}\text{Ti}(I=68, 88, 112 \hbar)$, and $^{48}\text{Cr}(I=72, 98, 120 \hbar)$, as shown in Fig. 3 and listed in Table I. Note that with a fixed initial shape of a ring of 10 alpha particles, the earlier result of [11] finds only a single case of $^{40}\text{Ca}(I=60 \hbar)$ as an isomeric toroidal figure of equilibrium. However, with the help of Fig. 1(b) and the fine grids in the large multi-dimensional space of (A, Q_{20}, I) , we find a large number of isomers, demonstrating the general occurrence of toroidal high-spin states. The A and I values have their correspondences in the (N, I) shells in Fig. 1(b). The equilibrium configurations at the energy minima have been tested and found to be self-consistently free-converging after the removal of the quadrupole moment Q_{20} constraint.

Table 1 gives the properties of the high-spin toroidal isomers in $28 \leq A \leq 48$: their Q_{20} , $\hbar\omega$, and excitation en-

ergy E^* values, obtained with the Skyrme SkM* interaction. The excitation energy is of order 140-270 MeV. The toroidal density can be parametrized as a Gaussian function, $\rho(r, z) = \rho_{\text{max}} \exp\{-[(r - R)^2 + z^2]/(d^2/\ln 2)\}$, where R , d , and ρ_{max} for isomeric states are listed. While the major radius R and R/d increase with increasing A , the minor radius d remains to be approximately the same.

Table 1: Properties of high-spin toroidal isomers at their local energy minima in $28 \leq A \leq 48$.

	I/\hbar	Q_{20} (b)	$\hbar\omega$ (MeV)	E^* (MeV)	R (fm)	d (fm)	R/d	ρ_{max} (fm $^{-3}$)
^{28}Si	44	-5.86	2.8	143.18	4.33	1.45	2.99	0.119
^{32}S	48	-8.22	1.9	153.87	4.87	1.42	3.43	0.122
	66	-10.51	2.2	193.35	5.57	1.40	3.98	0.108
^{36}Ar	56	-11.31	1.7	168.03	5.44	1.40	3.88	0.125
	72	-13.73	1.85	198.63	6.04	1.39	4.34	0.113
	92	-16.78	2.0	238.56	6.73	1.37	4.91	0.103
^{40}Ca	60	-14.96	1.5	178.36	5.97	1.40	4.26	0.126
	82	-17.61	1.9	214.23	6.51	1.39	4.68	0.117
^{44}Ti	68	-19.57	1.2	195.46	6.55	1.39	4.71	0.128
	88	-22.27	1.4	223.09	7.01	1.38	5.08	0.120
	112	-25.76	1.6	260.24	7.56	1.37	5.52	0.113
^{48}Cr	72	-25.08	1.2	207.12	7.12	1.38	5.16	0.128
	98	-28.00	1.4	239.26	7.54	1.37	5.50	0.122
	120	-30.55	1.43	271.02	7.90	1.36	5.81	0.118

We plot in Fig. 4 the density distributions of the toroidal configurations of ^{40}Ca with $I=60 \hbar$ as a cut in the radial x -direction for different Q_{20} . One notes that the average density for $^{40}\text{Ca}(I=60 \hbar)$ at the toroidal energy minimum of $Q_{20} = -15$ b (thick solid curve) is only 0.64 of the average nuclear density for a spherical ^{40}Ca (dash-dot curve). This is a general phenomenon for light toroidal nuclei, as the nuclear density is affected by the presence of all forces [22].

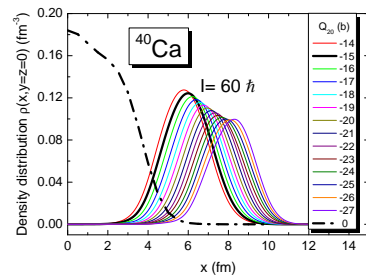


Figure 4: (Colour online.) The density distributions of ^{40}Ca for $I=60 \hbar$ as a cut in the radial direction x for different Q_{20} : (i) the thick solid curve is for the equilibrium toroidal configurations at the local energy minimum at $Q_{20} = -15$ b, (ii) the thin line curves are for the other Q_{20} as labelled, and (iii) the dashed-dot curve is for ^{40}Ca in the spherical ground state.

To gain new insights into the nature of the non-

collective rotational motion, we determine an effective moment of inertia $\mathfrak{J}_{\text{eff}}$ for toroidal ^{40}Ca from the total energy of the system as a function of I as $E^{\text{tot}}(I) = E^{\text{tot}}(0) + I(I+1)/2\mathfrak{J}_{\text{eff}}$. Using the results in Fig. 3, we find in Fig. 5(a) that such a linear dependence between $E^{\text{tot}}(I) - E^{\text{tot}}(0)$ and $I(I+1)$ holds for different Q_{20} . An effective moment of inertia $\mathfrak{J}_{\text{eff}}$ can be extracted as a function of Q_{20} . On the other hand, for different Q_{20} , one can calculate the rigid-body moment of inertia $\mathfrak{J}_{\text{rigid}} = m_N 2\pi^2 R(d^2/\ln 2)\rho_{\text{max}}[R^2 + 3/(2\ln 2)d^2]$ from the density distributions in Fig. 4. The comparison of $\mathfrak{J}_{\text{eff}}$ and $\mathfrak{J}_{\text{rigid}}$ in Fig. 5(b) indicates the approximate equality of $\mathfrak{J}_{\text{eff}}$ and $\mathfrak{J}_{\text{rigid}}$. This is in agreement with the result of Bohr and Mottelson who showed that the moment of inertia associated with the alignment of single-particle orbits along an axis of symmetry is equal to the rigid-body moment of inertia [23] and justifies the use of $\mathfrak{J}_{\text{rigid}}$ in the earlier liquid-drop model of a rotating toroidal nucleus in [7].

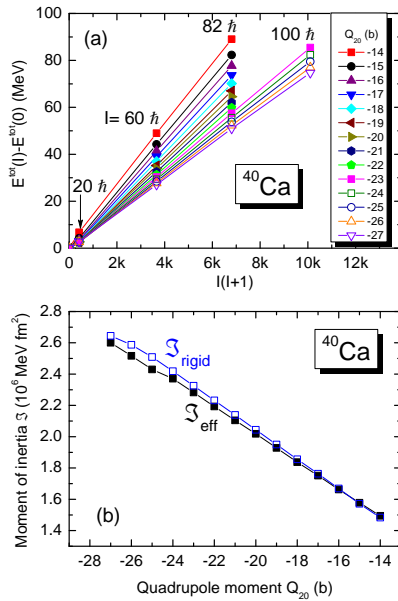


Figure 5: (Color online) (a) The total energy difference $E^{\text{tot}}(I) - E^{\text{tot}}(0)$ as a function of $I(I+1)$ for toroidal ^{40}Ca at different Q_{20} . The inverses of the slopes of different lines give the effective moments of inertia $\mathfrak{J}_{\text{eff}}$. (b) The effective moments of inertia $\mathfrak{J}_{\text{eff}}$ and the rigid body moments of inertia $\mathfrak{J}_{\text{rigid}}$ as a function of Q_{20} for toroidal ^{40}Ca .

It is clear from Fig. 1(b) that large shell effects are expected for some odd N and Z at various I values, and for combining different (N, I_N) with (Z, I_Z) at the same $\hbar\omega$. Hence light toroidal nuclei with odd- N , odd- Z , and $N \neq Z$ may be possible. The large shell gaps for

$(N, I)=(58, 58 \hbar)$, $(64, 32 \hbar)$, and $(64, 96 \hbar)$ calls for future exploration of high-spin toroidal isomers in the mass region of $A \sim 120$.

In conclusion, under the considerations of the aligned single-particle angular momentum and the bulk behaviour, the constrained self-consistent Skyrme-Hartree-Fock model calculations reveal that high-spin toroidal isomers may have general occurrences in the mass region of $28 \leq A \leq 48$. Experimental search for these nuclei may allow the extraction of the bulk properties of this new type of nuclear fluid and its possible utilization as a source of energy.

Acknowledgments

The authors wish to thank Drs. Jerzy Dudek, Vince Cianciolo, and I-Yang Lee for helpful discussions. This work was supported by the National Science Center (Poland) and in part by the Division of Nuclear Physics, U.S. Department of Energy.

References

- [1] See a reference to J. A. Wheeler's toroidal nucleus in G. Gamow, Biography of Physics, Harper & Brothers Publishers, N.Y. 1961, pp. 297.
- [2] C.Y. Wong, Phys. Lett. 41B (1972) 446-450.
- [3] C.Y. Wong, Ann. of Phys. (N.Y.) 77 (1973) 279-353.
- [4] G. Royer, F. Haddad, B. Jouault, Nucl. Phys. A 605 (1996) 403-416.
- [5] V. Zhrebchevsky *et al.* Phys. Lett. B 646 (2007) 12-18.
- [6] A. Staszczak, C.Y. Wong, Acta Phys. Pol. B 40 (2008) 753-757, and references cited therein.
- [7] C.Y. Wong, Phys. Rev. C 17 (1978) 331-340.
- [8] A. Bohr, B.R. Mottelson, Nucl. Phys. A 354 (1981) 303c-316c.
- [9] Ph. Eudes, Z. Basrak, F. Sébille, V. de la Mota, G. Royer, M. Zoric, J. Phys. Conf. Ser. 420 (2013) 012133-1-8.
- [10] H. Esbensen, Phys. Rev. C 85 (2012) 064611-1-9.
- [11] T. Ichikawa, J.A. Maruhn, N. Itagaki, K. Matsuyanagi, P.-G. Reinhard, S. Ohkubo, Phys. Rev. Lett. 109 (2012) 232503-1-4.
- [12] P. Ring, P. Schuck, The Nuclear Many-Body Problem, Springer-Verlag, Berlin, Heidelberg, New York, 1980, pp. 142.
- [13] M.J.A. de Voigt, J. Dudek, Z. Szymański, Rev. Mod. Phys. 55 (1983) 949-1046.
- [14] S.G. Nilsson, I. Ragnarsson, Shapes and Shells in Nuclear Structure, Cambridge University Press, 1995, pp. 223.
- [15] M. Brack, J. Damgaard, A.S. Jensen, H.C. Pauli, V.M. Strutinsky, C.Y. Wong, Rev. Mod. Phys. 44 (1972) 320-405.
- [16] D. Vautherin, D.M. Brink, Phys. Rev. C 5 (1972) 626; Y.M. Engel, D.M. Brink, K. Goeke, S. Krieger, D. Vautherin, Nucl. Phys. A 249 (1975) 215.
- [17] A. Staszczak, M. Stoitsov, A. Baran, W. Nazarewicz, Eur. J. Phys. A 46 (2010) 85-90.
- [18] N. Schunck *et al.* Comput. Phys. Commun. 183 (2012) 166-192.
- [19] J. Bartel, P. Quentin, M. Brack, C. Guet, H.B. Håkansson, Nucl. Phys. A 386 (1982) 79-100.
- [20] J. Dobaczewski, W. Nazarewicz, M.V. Stoitsov, Eur. J. Phys. A 15 (2002) 21-26.

- [21] A. Staszczak, A. Baran, J. Dobaczewski, W. Nazarewicz, Phys. Rev. C 80 (2009) 014309-1-6.
- [22] C.Y. Wong, Phys. Rev. Lett. 55 (1985) 1973-1975.
- [23] A. Bohr, B. R. Mottelson, Nuclear Structure. Vol. II: Nuclear Deformations, World Scientific, Singapore, New Jersey, Hong Kong, 1998, page 80.